Advances in Nano Research, *Vol. 16, No. 3 (2024) 251-263*
https://doi.org/10.12989/anr.2024.16.3.251

Analytical nonlocal elasticity solution and ANN approximate for free vibration response of layered carbon nanotube reinforced composite beams

Emrah Madenci*[1], Şaban Gülcü[2] and Kada Draiche[3,4]

[1]*Department of Civil Engineering, Necmettin Erbakan University, 42090 Konya, Türkiye*
[2]*Department of Computer Engineering, Necmettin Erbakan University, 42090 Konya, Türkiye*
[3]*Department of Civil Engineering, University of Tiaret, B.P. 78 Zaaroura, 14000 Tiaret, Algeria*
[4]*Material and Hydrology Laboratory, University of Sidi Bel Abbes, Faculty of Technology, Civil Engineering Department, Algeria*

(*Received January 20, 2022, Revised July 18, 2023, Accepted September 21, 2023*)

Abstract. This article investigates the free vibration behavior of carbon nanotube reinforced composite (CNTRC) beams embedded using variational analytical methods and artificial neural networks (ANN). The material properties of layered functionally graded CNTRC (FG-CNTRC) beams are estimated using nonlocal parameters modified power-law with different types of CNT distributions through the thickness direction of the beam. Adopting Eringen's nonlocal elasticity theory to capture the small size effects, the nonlocal governing equations are derived and solved using the analytical method. And also, the problem was analyzed using the ANN method. The architecture of the proposed ANN model is 3-9-1. In the experiments, we used 112 different data to predict the natural frequency using ANN. Based on the nonlocal differential constitutive relations of Eringen, the equations of motion as well as the boundary conditions of the beam are derived using Hamilton's principle. The classical beam theory is used to formulate a governing equation for predicting the free vibration of laminated CNTRC beams. According to the experimental results, the prediction ability of the ANN model is very good and the natural frequency can be predicted in ANN without attempting any experiments.
Keywords: artificial neural networks; carbon nanotube; composite beam; free vibration; nonlocal elasticity theory

1. Introduction

The carbon nanotubes (CNTs) have become utilized in many essential fields including engineering and have received attentions amid scientists. The application of CNT reinforcement structures in many industries is rising due to their excellent properties such as high strength, low weight, resistance to fatigue and are useable in continuous yarns (Jam and Kiani 2015, Khosravi *et al*. 2019a, b, Khaniki and Ghayesh 2020, Babaei *et al*. 2021, Madenci *et al*. 2023). The single-walled CNT has a cylindrical shape that is continuously extruded with a single sheet of graphene about 1 nm in diameter and centimeter long (Bourada *et al*. 2020). In contrast, multi-walled CNT has an array of such cylinders that are concentrically formed and separated by 0.35 nm, similar to basal plane separation in graphite with diameters of 2 nm to 100 nm and lengths of tens of microns (Asghar *et al*. 2020). In traditional methods, nanotubes are uniformly or randomly distributed, therefore, the improvement of their special mechanical properties may not be perfect (Qin *et al*. 2020). Nanotechnology and nanoscience are attractive research topics that have been taken into considerations in the past decades for this purpose (Kannan *et al*. 2012, Mirzaei and Kiani 2015, Khater and Abd el Gawaad 2016, Kumar 2018, Eltaher *et al*. 2019, Asghar *et al*. 2020, Hosseini and Khosravi 2020, Hussain *et al*. 2020a, b, c, Farazin and Mohammadimehr 2021).

Carbon nanotube reinforced composites (CNTRCs) are a new generation of composite materials in which the ratio of the two in-plane Young's modulus is more than 40 and the in-plane shear modulus is very small compared to the longitudinal Young's modulus (Shen *et al*. 2020). Therefore, the auxiliary CNTRC laminate is expected and the magnitude of the Poisson ratio can be increased in some directions. CNTRC laminated structures have potential use in the industry and engineering fields such as mechanical, civil, aerospace as load bearing instrument for ships, building and aircrafts, etc (Kiani 2016).

Methods such as atomistic modeling and continuum mechanics are used to understand the mechanical performance of CNTs (Eltaher *et al*. 2019). Eberhardt and Wallmersperger (2015) studied a modified molecular structural mechanics model to determine the elastic properties of CNTs. Ghadyani *et al*. (2016) proposed an algorithm based on a numerical finite element analysis, to relate the physical geometry to the elastic properties of asymmetric SWCNTs. Kumar (2018) presented mechanical vibration of double-walled carbon nanotubes with inter-tube Van der Waals forces.

In the literature, plenty of theories to analyze the small-scale effect, including surface effect, modified coupled stress method, nonlocal elasticity theory and nonlocal strain gradient theory. The small-scale effect is very important in nanoscale structures, so several dimension-dependent continuum models have been developed. However, the most used continuity theory to investigate small-scale structures

*Corresponding author, Professor,
E-mail: emadenci@erbakan.edu.tr

ISSN: 2287-237X (Print), 2287-2388 (Online)

is the nonlocal elasticity model proposed by Eringen (1983). The application of nonlocal elasticity in micro and nanomaterials has received much attention among the nanotechnology community recently. The nonlocal elasticity model is widely used in small-scale materials for bending, vibration and buckling analyzes of micro/nano structures (Bounouara *et al*. 2016, Mehar *et al*. 2016, Mouffoki *et al*. 2017, Karami *et al*. 2018, Youcef *et al*. 2018). Aydogdu (2012) applied nonlocal elasticity theory in axial vibration analysis of single-walled carbon nanotubes embedded in elastic medium. Şimşek and Yurtcu (2013) presented an analytical solution for bending and buckling of FG nanobeams using the nonlocal Timoshenko beam theory. Free vibration analysis of double walled carbon nanotubes (DWCNT) embedded in elastic medium with initial imperfection is investigated by Ehyaei and Daman (2017). Timoshenko beam theory is employed. However the nonlocal theory is used for modeling the nano scale of nanotube. In addition, the governing equations were obtained due to the Hamilton principle. Khosravi and Hosseini (2020) conducted the nonlocal model to investigate the small-scale torsional behavior of the single-walled CNTs for free case and for the state in which model is subjected to the linear and harmonic torques. Static bending and buckling of the FG porous nanoscale beam are investigated based on the nonlocal Timoshenko beam theory including neutral surface position by Bensaid and Guenanou (2017). Hosseini *et al*. (2020) investigated axial vibration of FG nanobeams using nonlocal elasticity theory under clamped-clamped and clamped-free boundary conditions. Power law, exponential law and sigmoid law were applied as grading laws to examine the effect of the material distribution on axial vibration of the FG nanobeams. Eltaher *et al*. (2016) investigated the effects of thermal load and shear force on the buckling of nanobeams. The nonlocal Eringen elasticity model was adopted to account a size-dependence at the nano-scale. A simple and refined nonlocal hyperbolic higher-order beam theory is proposed for bending and vibration response of nanoscale beams by Kheroubi *et al*. (2016). The large amplitude free vibrations of a sandwich beam with stiff core and CNTRC face sheets are analyzed by Mirzaei and Kiani (2016). The equivalent single- layer theory of Timoshenko is used to construct the Hamiltonian of the beam under the von Kármán type of geometrical nonlinearity assumptions.

Application of classical continuum theory to the analysis of nanostructures is inappropriate because classical theories lack accountability for size effects resulting from small scale. In classical elasticity theory, the stress at a point depends only on the strain at the same point, whereas in the nonlocal elasticity theory the stress at a point is a function of the strains at all points of the continuum (Wang and Li 2014). In this way, the nonlocal continuum theory contains information about the long-range forces between atoms, and the internal length scale is simply included as a material parameter in the constitutive equations to capture the small-scale effect. The propagation characteristics of the elastic wave in fluid-conveying double-walled carbon nanotubes are investigated by Wang *et al*. (2010). The nonlocal continuum theory is applied to discuss the dispersion relation with small scale effects. The effects of the viscous fluid on the propagation characteristics of elastic waves in carbon nanotubes are studied Wang *et al*. (2011). Based on the nonlocal continuum theory, the small scales effects are also considered. Numerical simulations are performed with the consideration of different scale coefficients to discuss the influence of the viscous fluid. Thai and Vo (2012) proposed a nonlocal shear deformation beam theory for bending, buckling and vibration of homogeneous nanobeams based on Eringen's nonlocal elasticity theory. The effects of the axial load and the elastic matrix on the flexural wave in the carbon nanotube are studied by Wang *et al*. (2012). Based on the nonlocal continuum theory and the Timoshenko beam model, the equation of the flexural wave motion is derived. The dispersion relation between the frequency and the wave number is illustrated. Ebrahimi and Barati (2016) investigated the buckling behavior of shear deformable piezoelectric nanoscale beams made of functionally graded materials embedded in Winkler-Pasternak elastic medium and subjected to an electro-magnetic field. To consider the small size effects, Eringen's nonlocal elasticity theory was adopted. This article investigates the vibration behavior of magneto-electro-elastic functionally graded nanobeams embedded in a two-parameter elastic foundation using a third-order parabolic shear deformation beam theory. Based on Eringen's nonlocal elasticity theory which captures the small size effects and using the Hamilton's principle, the nonlocal governing equations of motions were derived and then solved analytically. A new nonlocal higher order shear deformation theory was developed for buckling properties of a single graphene sheet by Bouadi *et al*. (2018). The proposed nonlocal higher order shear deformation theory contains a new displacement field which incorporates undetermined integral terms and contains only two variables. The length scale parameter was considered in the present formulation by employing the nonlocal differential constitutive relations of Eringen. Mokhtar *et al*. (2018) presented a novel shear deformation theory for buckling analysis of single-layer graphene sheet based on nonlocal elasticity theory.

Experimental simulations on nanostructures are difficult, so some researchers studied and reported theoretical analyses of CNTRC structures using classical theories such as Euler-Bernoulli, Kirchhoff etc. and first order/high order shear deformation theories (Shekari *et al*. 2017, Chavan and Lal 2018, Ebrahimi and Farazmandnia 2018). Madenci (2021) presented efficient energy functional for CNTRC nanobeams based on high order shear deformation theory via mixed finite element method. Madenci and Gülcü (2020) proposed a model based on artificial neural networks was performed well for the maximum displacement of FGM beams such as Young modulus ratio, length to thickness ratio, the effect of the shear correction factor, effect of the power-low exponent. Ebrahimi and Barati (2018) presented an analytical solution of FG piezoelectric nanobeams by using a developed third-order shear deformation theory. Duc *et al*. (2018) investigated dynamic analysis of imperfect rectangular nanocomposite multilayer organic solar cells using the classical plate theory. Wu *et al*. (2015)

examined the free vibration and buckling behavior of sandwich beams reinforced with FG-CNTRCs face sheets based on Timoshenko beam theory. A new nonlocal higher order shear deformation theory is developed for buckling properties of a single graphene sheet by Bouadi *et al*. (2018). A new nonlocal higher order shear deformation theory was developed for buckling properties of a single graphene sheet by Bouadi *et al*. (2018). The proposed nonlocal higher order theory contains a new displacement field that incorporates undetermined integral terms and contains only two variables. An important and important issue in fiber reinforced polymer (FRP) composites is the reinforcement of the interlayer region. The properties of the regions between weak layers limit the overall performance of laminated FRP composite structures. In FGMs, the change of material properties has a functional transition. So there is no delamination problem (Uyaner and Yar 2019, Vedernikov *et al*. 2020, Alajarmeh *et al*. 2021, Korotkov *et al*. 2021, Madenci 2023).

Recently soft computing techniques such as artificial neural networks (ANNs), genetic algorithm and fuzzy logic have been used extensively for damage assessment with varied success (Hakim and Razak 2013). ANNs, inspired by the human brain, are powerful tools used to solve many real-life problems, which are considered a powerful method in the field of structural dynamics. ANNs are usually employed when the relationship between the input and output is complicated or if the application of another available method takes a large amount of computational time and if the effort is very expensive. Gülcü (2021) developed an ANN model to predict the compressive strength of the rubberized concrete. On the other hand, there are not enough applications of ANNs on the analysis of nanostructures in the literature.

In this study, analytical solutions for free vibration of CNTRC nanobeams with arbitrary boundary conditions considering the nonlocal parameter and ANN approximate are presented. The material properties of FG- CNTRCs are assumed to be graded through the thickness direction according to several distributions namely UD, FG-X, FG-V and FG-O. This distribution forms are given in Table 1. In ANNs approach, the ANN model was created by taking into account the natural frequency of the program and various key parameters that may affect its testing. The use of ANN modeling to analyze the free vibration of layered FG-CNTRC beams was validated by performing comprehensive convergence studies. The analytical and ANNs solutions for vibration analysis demonstrated the effects of nonlocal parameter, CNT distribution, layer angle and boundary conditions.

2. Formulation

The optimal design of beams has an important role in the development of nanotechnology. The mechanical parameters including maximum deflection and stress, buckling load and frequency responses are selected as design variables in different applications. In this section, exact solutions for the vibration behavior of CNTRC beams with arbitrary boundary conditions are developed which can be used in the conceptual design.

2.1 Nonlocal elasticity theory

The nonlocal theory of elasticity assumes that the stress at a point is related not only to the strain at that point but also to strains at all other points of the body. In the non-local elasticity, the uniaxial constitutive law is expressed as elasticity. The nonlocal stress tensor at the point is given by Eringen (1983)

$$\sigma^{nl}(x) = \int_{\Omega} K(|x' - x|, \tau) T(x')\, d\Omega(x') \tag{1a}$$

$$T(x) = C(x) : \varepsilon(x) \tag{1b}$$

where the macroscopic stress tensor at a point "**x**" is represented by "*T*" and depends on the strain at the same point which is based on the generalized Hook's law. "*C*" is the fourth-order elasticity tensor which represents the double-dot product. The kernel function "$K(|x' - x|, \tau)$" denotes the nonlocal modulus, (**x**'−**x**) indicates the distance and "τ" is the material constant which depends on the type of material, "$\varepsilon(x)$" is the strain tensor. "τ" is the material constant which is defined as "$\tau = \frac{e_0 \alpha}{l}$" and where "$e_0$" is a constant appropriate to each material, "*α" is an* internal characteristics length and "*l"* is an external characteristics length. In general, a conservative estimate of the nonlocal parameter is "$e_0\alpha$ < 2.0 nm" for a single-walled CNT (Tounsi *et al*. 2013). Since the solution of the constituent equation in integral form is complex, a simplified differential form equation can be used as given below

$$\begin{aligned} &L\sigma^{nl}(x) = (1 - \mu\nabla^2)\sigma^{nl} = T \\ &\mu = \tau^2 l^2 \end{aligned} \tag{2}$$

where "L^2" is the Laplacian operator and "$L = (1 - \mu\nabla^2)$" indicates nonlocal differential. The nonlocal parameter which is represented by "μ" varies in accordance with different materials. The nonlocal behavior can be neglected in the thickness direction for a beam type structure.

The nonlocal constitutive relation takes the following form based on classical beam theory

$$\sigma_{xx} - \mu \frac{\partial^2 \sigma_{xx}}{\partial x^2} = E(z)\varepsilon_{xx} \tag{3}$$

2.2 Governing equations

The displacement field of classical beam theory can be expressed as

$$\begin{aligned} &u(x,z,t) = u_0(x,t) - z\frac{\partial w_0}{\partial x} \\ &v(x,z,t) = 0 \\ &w(x,z,t) = w_0 \end{aligned} \tag{4}$$

The strain field of the beam is obtained as

$$V_{NP} = \frac{W_{NP}}{W_{NP} + (\rho_{NP}/\rho_M) - (\rho_{NP}/\rho_M)W_{NP}}, \tag{10}$$

where W_{NP} is the weight fraction of nanoparticles. The potential and kinetic energies of the structure are:

$$\varepsilon_{xx} = \varepsilon_{xx}^0 - z\kappa_x \tag{5}$$

where

$$\varepsilon_{xx}^0 = \frac{\partial u}{\partial x}; \quad \kappa_x = \frac{\partial^2 w_0}{\partial x^2} \tag{6}$$

To obtain the equations of motion, the expression for the Hamilton's principle of a CNTRC beam can be written as

$$\int_{T(time)} (\delta U + \delta V - \delta K) dT = 0 \tag{7}$$

where "δU" is the virtual variation of the total strain energy, "δV" is the virtual work and "δK" is the virtual kinetic energy, which are obtained as

$$\begin{aligned} \delta U &= \int_0^L \int_A \sigma_{xx} \delta \varepsilon_{xx} dA dx \\ &= \int_0^L (N_x \delta \varepsilon_{xx}^0 - M_x \delta \kappa_x) dx \end{aligned} \tag{8}$$

$$\delta V = -\int_0^L \left(q\delta w_0 + N_{x0} \frac{\partial w_0}{\partial x} \frac{\partial \delta w_0}{\partial x} \right) dx \tag{9}$$

$$\begin{aligned} \delta K &= \int_0^L \int_A \rho(z)[u\delta u + w\delta w]\, dA dx \\ &= \int_0^L \begin{bmatrix} I_0(u_0 \delta u_0 + w_0) + I_1 \left(u_0 \frac{\partial \delta w_0}{\partial x} + \frac{\partial w_0}{\partial x} \delta u_0 \right) \\ + I_2 \frac{\partial w_0}{\partial x} \frac{\partial \delta w_0}{\partial x} \end{bmatrix} dx \end{aligned} \tag{10}$$

The mass moment of inertia can be represented as

$$\begin{Bmatrix} I_0 \\ I_1 \\ I_2 \end{Bmatrix} = \int_A \rho(z) \begin{Bmatrix} 1 \\ z \\ z^2 \end{Bmatrix} dA \tag{11}$$

The "N_x" is the force resultant and the "M_x" is the moment resultant that they are defined as below

$$N_x = \int_A \sigma_{xx} dA \tag{12a}$$

$$M_x = \int_A z\sigma_{xx} dA \tag{12b}$$

Substituting Eqs. (8)-(10) into Eq. (7), integrating by parts and setting the coefficient "δu_0" and "δw_0" to zero lead to the following Euler-Lagrange equations:

$$\frac{\partial N}{\partial x} + f = 0 \tag{13a}$$

$$\frac{\partial^2 M_x}{\partial x^2} - q = 0 \tag{13b}$$

By using Eqs. (3), (5) and (12), the force-strain and the moment-strain relations of the nonlocal classical beam theory can be obtained as

$$N - \mu \frac{\partial^2 N}{\partial x^2} = A_{xx} \frac{\partial u}{\partial x} - B_{xx} \frac{\partial^2 w}{\partial x^2} \tag{14a}$$

Table 1 Volume fraction and distribution forms of CNT

Distribution form	Volume fraction
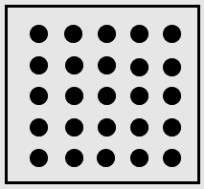	$UD: \quad V_{CNT}(z) = V_{CNT}^*$
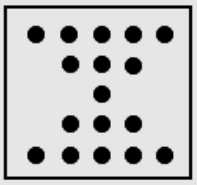	$XD: \quad V_{CNT}(z) = \frac{4\lvert z\rvert}{h} V_{CNT}^*$
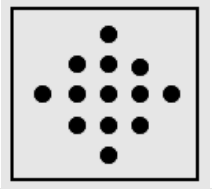	$OD: \quad V_{CNT}(z) = 2\left(1 - \frac{2\lvert z\rvert}{h}\right) V_{CNT}^*$
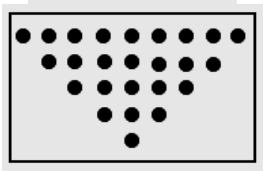	$VD: \quad V_{CNT}(z) = \left(1 + \frac{2\lvert z\rvert}{h}\right) V_{CNT}^*$

$$M_x - \mu \frac{\partial^2 M_x}{\partial x^2} = B_{xx} \frac{\partial u}{\partial x} - D_{xx} \frac{\partial^2 w}{\partial x^2} \tag{14b}$$

where the following cross-sectional rigidities are defined as

$$(A_{xx}, B_{xx}, D_{xx}) = \int_A E(z)(1, z, z^2) dA \tag{15}$$

2.3 CNTRC micro-mechanic model

The effective material properties of the two phase composites, the mixture of CNTs and an isotropic polymer, can be determined from the rule of the mixture as

$$E_{11} = \eta_1 V_{CNT} E_{11}^{CNT} + V_m E_m \tag{16}$$

$$\frac{\eta_2}{E_{22}} = \frac{V_{CNT}}{E_{22}^{CNT}} + \frac{V_m}{E_m} \tag{17}$$

$$\frac{\eta_3}{G_{12}} = \frac{V_{CNT}}{G_{12}^{CNT}} + \frac{V_m}{G_m} \tag{18}$$

$$\upsilon_{12} = V_{CNT} \upsilon_{12}^{CNT} + V_m \upsilon_m \tag{19}$$

$$\rho = V_{CNT} \rho_{CNT} + V_m \rho_m \tag{20}$$

where "E_{11}^{CNT}, E_{22}^{CNT} and G_{12}^{CNT}" are Elasticity modulus and shear modulus of CNT, "E_m and G_m" are elasticity and shear modulus of the isotropic matrix, "η_1, η_2 and η_3" are CNT/matrix efficiency parameters, "υ_{12}^{CNT} and υ_m" are Poisson's ratios of CNT and matrix, "ρ_{CNT} and ρ_m" are mass densities of CNT and matrix, respectively. Also,

"V_{CNT}" and "V_m" are volume fractions of CNT and matrix, respectively and related by

$$V_{CNT} + V_m = 1 \tag{21}$$

where "V^*_{CNT}" is the volume fraction of CNT that is determined by

$$V^*_{CNT} = \frac{w_{CNT}}{w_{CNT} + \frac{\rho_{CNT}}{\rho_m} - \frac{\rho_{CNT}}{\rho_m} w_{CNT}} \tag{22}$$

where "w_{CNT}" is the mass fraction of CNT.

The nonlocal constitutive relations for the *k*th layer of the CNTRC beam take the form

$$\sigma^{(k)}_{xx} - \mu \frac{\partial^2 \sigma^{(k)}_{xx}}{\partial x^2} = \bar{Q}^{(k)}_{11}(z)\varepsilon^{(k)}_{xx} \tag{23}$$

where

$$\begin{aligned} \bar{Q}^{(k)}_{11} &= Q^{(k)}_{11}(z)\, cos^4\theta \\ &+2\left(Q^{(k)}_{12}(z) + 2Q^{(k)}_{66}(z)\right) sin^2\theta\, cos^2\theta \\ &+Q^{(k)}_{22}(z)\, sin^4\theta \end{aligned} \tag{24}$$

$$\begin{aligned} Q^{(k)}_{11}(z) &= \frac{E^{(k)}_{11}(z)}{1 - \upsilon^{(k)}_{12}(z)\upsilon^{(k)}_{21}(z)}; \\ Q^{(k)}_{21}(z) &= \frac{\upsilon^{(k)}_{12}(z)E^{(k)}_{22}(z)}{1 - \upsilon^{(k)}_{12}(z)\upsilon^{(k)}_{21}(z)} \\ Q^{(k)}_{22}(z) &= \frac{E^{(k)}_{22}(z)}{1 - \upsilon^{(k)}_{12}(z)\upsilon^{(k)}_{21}(z)}; \\ Q^{(k)}_{66}(z) &= G^{(k)}_{12}(z) \end{aligned} \tag{25}$$

These parameters depend on the CNT volume fraction of the *k*th layer.

2.4 Analytical solution

The nonlocal axial normal force and bending moment can be written as

$$N = A_{xx}\frac{\partial u}{\partial x} - B_{xx}\frac{\partial^2 w}{\partial x^2} - \mu\frac{\partial^2 f}{\partial x} \tag{26a}$$

$$M_x = B_{xx}\frac{\partial u}{\partial x} - D_{xx}\frac{\partial^2 w}{\partial x^2} + \mu\left(\frac{\partial^2 w}{\partial x^2}\bar{N} - q\right) \tag{26b}$$

The nonlocal governing equations in terms of the displacements can be obtained by substituting for *N*, *M* from Eqs. (26a, b), respectively, into Eqs. (14a, b) as follows:

$$A_{xx}\frac{\partial^2 u}{\partial x^2} - B_{xx}\frac{\partial^3 w}{\partial x^3} = \mu\frac{\partial^2 f}{\partial x} - f \tag{27a}$$

$$B_{xx}\frac{\partial^3 u}{\partial x^3} - D_{xx}\frac{\partial^4 w}{\partial x^4} - \bar{N}\frac{\partial^2 w}{\partial x^2} + \mu\bar{N}\frac{\partial^2 w}{\partial x^2} = \mu\frac{\partial^2 q}{\partial x^2} - q \tag{27b}$$

The exact solution of natural vibration of CNTRC beam was considered and the boundary conditions are

$$SS \rightarrow \underset{x=L}{w_{x=0}} = 0 \qquad \underset{x=L}{M_{x=0}} = 0 \tag{28}$$

$$\begin{aligned} CC &\rightarrow \underset{x=L}{w_{x=0}} = 0 \\ CF &\rightarrow w_{x=0} = 0 \qquad M_{x=L} = 0 \\ CS &\rightarrow \underset{x=L}{w_{x=0}} = 0 \qquad M_{x=L} = 0 \end{aligned}$$

The following expansions of the generalized displacements satisfy the boundary conditions

$$W(x,t) = \sum_{n=1}^{\infty} W_n\, sin\frac{n\pi x}{L} e^{i\omega_n t} \tag{29}$$

The general solution is

$$\begin{aligned} W(x) = c_1\, sin\,\lambda\, x + c_2\, cos\,\lambda\, x + c_3\, sin\hbar\, u\, x \\ + c_4\, cos\hbar\, u\, x \end{aligned} \tag{30}$$

where "c_1, c_2, c_3 and c_4" are integration constants, which must be evaluated using the boundary conditions.

The natural frequencies are given by

$$\begin{aligned} \omega^2 &= \frac{1}{\lambda M_x}\left(\frac{\eta\pi}{L}\right)^4 E(z)I_{xx} \\ \lambda &= 1 + \mu\left(\frac{n\pi}{L}\right)^2 \end{aligned} \tag{31}$$

For free vibration, we set "$\bar{N}$" and "q" to zero.

2.5 Artificial Neural Networks (ANNs)

Artificial Neural Networks (ANNs) is a technology that is inspired by the biological nervous system and performs the learning feature, which is the most important feature of the human brain. The learning feature refers to the ability of a neural network to make certain inferences as a result of its experiences. ANN learns from examples and makes decisions about the examples they encounter later using their previous knowledge. Thus, it makes generalizations about new examples. ANN has been successfully used in many different areas such as agriculture (Eldem 2020), civil engineering (Madenci and Gülcü 2020), chemical engineering (Tümer *et al*. 2020), and many different problems such as the classification of type 2 diabetes (Frimpong *et al*. 2021), human gender prediction (Hacibeyoglu and Ibrahim 2018), and optimization of traffic signal timing (Karaşahin and Tümer).

Many ANN models have been proposed in the literature. A few of them are feed-forward artificial neural network (FFNN) (Bebis and Georgiopoulos 1994), Kohonen self-organizing network (Kohonen 1982), radial basis function network (Park and Sandberg 1993), recurrent neural network (Dorffner 1996). The most widely used model of these is the FFNN model.

FFNN consists of a series of data processing elements called neurons. Neurons are connected to each other and are located in units called layers. The first of these layers is called the input layer. The input layer maps the input data of the problem to the network by passing it on to the neurons. The last layer in the network structure is called the output layer. The layer between the input layer and the output layer is called the hidden layer. The number of hidden layers in the network and the number of neurons in the layers may differ depending on the difficulty level of the problem. The

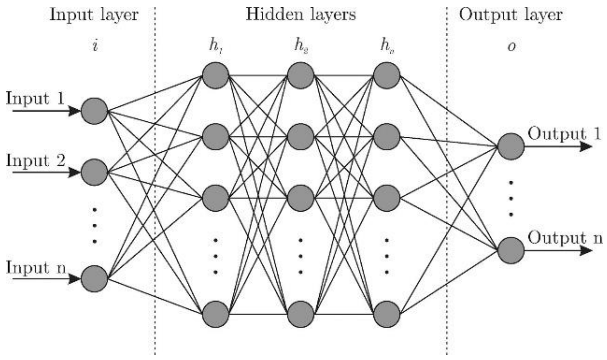

Fig. 1 The general architecture of the FFNN (Bre *et al*. 2018)

Table 2 Dataset properties used in the experiments

CNT Distribution model	Boundary Conditions	Fiber Angels
UD	SS	0º
XD	CC	15º
OD	CF	30º
VD	SC	45º
		60º
		75º
		90º

Table 3 Statistical analysis of data

Attribute	Min	Max	Mean	St. Dev.
CNT Distribution model	1	4	2.5	1.12
Boundary Conditions	1	4	2.5	1.12
Fiber Angels	1	7	4	2.01
Natural frequencies	0.0716	1.5147	0.6458	0.44

connections that allow neurons to connect to each other are called weights.

The general architecture of the FFNN is shown in Fig. 1. The outputs of neurons in a layer are given as inputs to the neurons in the next layer by passing through the weights. Information in the network is transferred in one direction from the input layer to the output layer. The performance of FFNN depends on the updating of the network with optimum values of the weights and biases.

The output of the FFNN with one hidden layer is calculated as follows (Mirjalili 2015, Gülcü 2020): The inputs, the initial values of weights, and biases are given to the network. In the first stage, the weighted sum value of the input is calculated by multiplying the input data and the connection weights between the input layer and hidden layer. Eq. (32) shows the weighted sum calculation.

$$t_i = \sum_{k=1}^{m} (A_{ki} * G_k) - \beta_i \qquad i = 1,2,\dots,n \tag{32}$$

where "*m*, *n*, *k*, and *i*" represent the total number of neurons in the input layer, the total number of neurons in the hidden layer, a neuron in the input layer, and a neuron in the hidden layer, respectively. "A_{ki}" represents the weight between the *k*th neuron in the input layer and the "*i*th" neuron in the hidden layer. "G_k" represents the input data. "β_i" represents the bias value of the "*i*th" neuron in the hidden layer. The output of each neuron in the hidden layer is calculated by the sigmoid function shown in Eq. (33).

$$T_i = Sigmoid(t_i) = \frac{1}{1 + e^{-t_i}} \tag{33}$$

where i and t_i represent a neuron in the hidden layer and the weighted sum calculation of the *i*th neuron, respectively. Eqs. (34) and (35) are used to calculate the actual output of the network.

$$c_y = \sum_{k=1}^{m} (A_{iy} * T_i) - \beta_y \qquad y = 1,2,\dots,p \tag{34}$$

$$C_y = Sigmoid(c_y) = \frac{1}{1 + e^{-c_y}} \tag{35}$$

where *n*, *p*, *i*, and *y* represent the total number of neurons in the hidden layer, the total number of neurons in the output layer, a neuron in the hidden layer, and a neuron in the output layer, respectively. A_{iy} represents the weight between *i*th neuron in the hidden layer and *y*th neuron in the output layer. T_i represents the output of the *i*th neuron in the hidden layer. β_y represents the bias value of the *y*th neuron in the output layer. c_y represents the weighted sum calculation of the *y*th neuron. C_y represents the output of the network. There are six fundamental steps in the application of FFNN: collecting and preparing data, defining network architecture, initializing weights and biases, training network, validating network, and using the network.

Collecting and preparing data is the first step of the application of the FFNN. Therefore, data should be coherent and should not contain missing values. To create a good neural network, 112 different design mixed data-set was obtained based on free vibration analysis of CNTRC layered beam. Where the input data are CNT distribution models, boundary conditions and fiber angels; output data is natural frequencies, respectively. The combination parameters of input data are given in Table 2.

The statistical analysis of the data is shown in Table 3.

In the step of preparing data, the instances of the training dataset, the validation dataset, and the test dataset are randomly determined. In the application of FFNN, a common task is the construction of a suitable model that can learn from data and make predictions on data. The data used to build the final model usually comes from multiple datasets. In particular, three datasets are commonly used in different stages of the creation of the model. They are the training dataset, the validating dataset, and the test dataset. The training dataset is a set of examples used to fit the weights and biases of the model. FFNN is trained using the training dataset to create the fittest model. Successively, the fitted model is used to predict the responses for the observations in a second dataset called the validation dataset (James *et al*. 2013). Finally, the test dataset is used to provide an unbiased evaluation of a final model fit on the training dataset. In general, the training data, the validation data, and the test data are 70%, 15%, and 15% of the data, respectively. In this paper, we also used the same

fragmentation. In addition, all data sets are normalized by using the min-max normalization function given in Eq. (36) to eliminate the effect of attributes that may have different effective rates on the classification (Aljarah *et al*. 2018).

$$x' = \frac{(x - x_{min})}{(x_{max} - x_{min})} \tag{36}$$

where x' represents the normalized form of *x*.

An FFNN contains one input layer, one or many hidden layers, and one output layer. In this study, we used the architecture of the FFNN with one hidden layer. Each layer contains one or many neurons depends on the problem. The input layer and the output layer have three neurons and one neuron respectively since the dataset used in the experiments contains three input and one output. There is no fixed rule in determining the number of neurons in the hidden layer. The number of neurons in the hidden layer is empirically determined using the validation dataset. In this study, the number of hidden neurons was started at two and was tried up to ten. Therefore, nine different FFNN architectures were used to determine the best model. The values of the weights and biases affect the performance of the FFNN. The values of the weights and biases are randomly initialized at the beginning of the algorithm. There is no fixed rule in initializing the values of the weights and biases. But they are often initialized in the range [-0.5, 0.5] or [-1, 1]. Therefore, they are initialized between -1 and 1 in this study.

In the training network, FFNN is trained using the training dataset which is 70% of the data in this study. The weights and biases of FFNN are optimized according to the inputs-outputs pattern in the training dataset. In this study, the mean square error (MSE) was used as the objective function whose formulation is given in Eq. (37). The aim is to minimize the MSE. In this study, the number of hidden neurons was started at two and was tried up to ten. Therefore, nine different FFNN architectures were used to determine the best model. At the end of the training network phase, nine models with the minimum MSE are created. Successively, the best model among nine models is found using the validation dataset. Finally, the test dataset is used to provide an unbiased evaluation of the best model fit on the training dataset. Thus, the best model is ready to use.

To evaluate the performance of FFNN, the statistical metrics which are frequently used in literature were applied. These statistical metrics are the MSE, the correlation of the coefficient (R), and the mean absolute error (MAE). Their formulations are shown in Eqs. (37)-(39).

$$MSE = \frac{\left(\sum_{i=1}^{N}(O_i - P_i)^2\right)}{N} \tag{37}$$

$$MAE = \frac{\left(\sum_{i=1}^{N}|O_i - P_i|\right)}{N} \tag{38}$$

$$R = \sqrt{1 - \left(\frac{\sum_{i=1}^{N}(O_i - P_i)^2}{\sum_{i=1}^{N}(O_i - \bar{P})^2}\right)} \tag{39}$$

where *N*, *O*, *P*, and $\bar{P}$ are the number of instances in the dataset, the observed value, the predicted value, and the mean of the predicted values, respectively.

Table 4 Material parameters of a CNTRC beam

Parameters	CNT	Matrix
Young's modulus	$E_{11} = 600$ GPa, $E_{22} = 10$ GPa	$E = 2.5$ GPa
Poisson's coefficient	$\nu = 0.3$	$\nu_{12} = 0.19$
mass density	$\rho = 1400$ kg/m^3	$\rho = 1190$ kg/m^3
shear modulus	$G_{12} = 17.2$ GPa	---

Table 5 The CNT efficiency parameters

V_{CNT}^*	η_1	η_2	η_3
0.12	1.2833	1.0556	1.0556
0.17	1.3414	1.7101	1.7101
0.28	1.3238	1.7380	1.7380
shear modulus	$G_{12} = 17.2$ GPa	---	

3. Numerical results

For the first comparison study, the fundamental frequency parameter of the layered CNTRC beam is evaluated and compared with literature results. The material properties of the CNTRC beam are given in Table 4.

The CNT efficiency parameters "η_i" associated with the given volume fraction "V_{CNT}^*" are shown in Table 5. It should be mentioned that the UD and other FG-CNT distributions nanobeams have the same mass fraction of CNT.

The non-dimensional parameter is defined as

$$\bar{\omega} = \omega \frac{L^2}{h}\sqrt{\frac{\rho_m}{E_m}} \tag{40}$$

Tables 6-9 provide the non-dimensional natural frequencies of four-layered simply-supported (SS) angle-ply CNTRC beams by the classical and nonlocal theories are compared for different distributions of CNTs for V_{CNT}^*=0.12 case. Frequency values started to decrease with the increase of nonlocal parameter. Considering the effect of the layer angle, the frequency value decreased with the increase of the angle. CNT distribution had an effect on frequency. While the lowest frequency value was in the FG-O distribution, the highest frequency value occurred in the FG-X distribution. The results are also presented for different boundary condition cases. Tables 10-13 give the results for the clambed-clamb (CC) boundary condition. Compared to the SS support, the CC support results were lower. Frequency values decreased with the increase of nonlocal parameter and angle. The frequency values of the cantilever beam are given in Tables 14-17. Due to the boundary conditions, the frequency values decreased significantly. The frequency results of beams with CS boundary condition are presented in Tables 18-21. The frequency values for the CS beam were close to the results of the CC beam. In addition, the results were compared with the mixed finite element solution results made by Madenci (2021) and the local results where the u parameter was 0, and the results were the same.

Table 6 The non-dimensional natural frequencies of SS CNTRC beams for UD distributions

μ	0º	15º	30º	45º	60º	75º	90º
0	0.9748	0.9281	0.7886	0.5715	0.3417	0.2139	0.2003
2	0.8899	0.8473	0.7199	0.5217	0.3119	0.1952	0.1828
4	0.8133	0.7743	0.6579	0.4768	0.2850	0.1784	0.1671
(Madenci 2021)	0.9748	0.9281	0.7886	0.5715	0.3417	0.2139	0.2003

Table 7 The non-dimensional natural frequencies of SS CNTRC beams for FG-X distributions

μ	0º	15º	30º	45º	60º	75º	90º
0	0.9851	0.9382	0.7976	0.5782	0.3452	0.2149	0.2009
2	0.8993	0.8565	0.7282	0.5278	0.3151	0.1962	0.1834
4	0.8219	0.7827	0.6654	0.4824	0.2880	0.1793	0.1676
(Madenci 2021)	0.9851	0.9382	0.7976	0.5782	0.3452	0.2149	0.2009

Table 8 The non-dimensional natural frequencies of SS CNTRC beams for FG-V distributions

μ	0º	15º	30º	45º	60º	75º	90º
0	0.9733	0.9266	0.787	0.5703	0.3413	0.2142	0.2006
2	0.8886	0.8459	0.7185	0.5206	0.3116	0.1955	0.1831
4	0.8120	0.7730	0.6566	0.4757	0.2847	0.1786	0.1673
(Madenci 2021)	0.9733	0.9266	0.787	0.5703	0.3413	0.2142	0.2006

Table 9 The non-dimensional natural frequencies of SS CNTRC beams for FG-O distributions

μ	0º	15º	30º	45º	60º	75º	90º
0	0.9639	0.9174	0.7785	0.5638	0.3381	0.2135	0.2003
2	0.8800	0.8375	0.7107	0.5147	0.3086	0.1949	0.1828
4	0.8041	0.7654	0.6495	0.4704	0.2821	0.1781	0.1671
(Madenci 2021)	0.9639	0.9174	0.7785	0.5638	0.3381	0.2135	0.2003

Table 10 The non-dimensional natural frequencies of CC CNTRC beams for UD distributions

μ	0º	15º	30º	45º	60º	75º	90º
0	1.5052	1.4710	1.3507	1.0985	0.7265	0.4729	0.4441
2	1.3742	1.3430	1.2331	1.0029	0.6632	0.4317	0.4054
4	1.2558	1.2273	1.1269	0.9165	0.6061	0.3945	0.3705
(Madenci 2021)	1.5052	1.4710	1.3507	1.0985	0.7265	0.4729	0.4441

Table 11 The non-dimensional natural frequencies of CC CNTRC beams for FG-X distributions

μ	0º	15º	30º	45º	60º	75º	90º
0	1.5147	1.4807	1.361	1.1086	0.7332	0.4749	0.4454
2	1.3829	1.3518	1.2425	1.0121	0.6694	0.4335	0.4066
4	1.2637	1.2354	1.1355	0.9249	0.6117	0.3962	0.3716
(Madenci 2021)	1.5147	1.4807	1.361	1.1086	0.7332	0.4749	0.4454

Table 12 The non-dimensional natural frequencies of CC CNTRC beams for FG-V distributions

μ	0º	15º	30º	45º	60º	75º	90º
0	1.5024	1.4677	1.346	1.0928	0.7235	0.4733	0.4448
2	1.3716	1.3400	1.2288	0.9977	0.6605	0.4321	0.4061
4	1.2535	1.2245	1.1230	0.9117	0.6036	0.3948	0.3711
(Madenci 2021)	1.5024	1.4677	1.346	1.0928	0.7235	0.4733	0.4448

Table 13 The non-dimensional natural frequencies of CC CNTRC beams for FG-O distributions

μ	0º	15º	30º	45º	60º	75º	90º
0	1.4997	1.4647	1.3425	1.0888	0.7199	0.4721	0.4442
2	1.3692	1.3372	1.2257	0.9940	0.6572	0.4310	0.4055
4	1.2512	1.2220	1.1201	0.9084	0.6006	0.3938	0.3706
(Madenci 2021)	1.4997	1.4647	1.3425	1.0888	0.7199	0.4721	0.4442

Table 14 The non-dimensional natural frequencies of CF CNTRC beams for UD distributions

μ	0º	15º	30º	45º	60º	75º	90º
0	0.3761	0.3553	0.2956	0.209	0.1229	0.0765	0.0716
2	0.3433	0.3243	0.2698	0.1908	0.1122	0.0698	0.0653
4	0.3138	0.2964	0.2466	0.1743	0.1025	0.0638	0.0597
(Madenci 2021)	0.3761	0.3553	0.2956	0.209	0.1229	0.0765	0.0716

Table 15 The non-dimensional natural frequencies of CF CNTRC beams for FG-X distributions

μ	0º	15º	30º	45º	60º	75º	90º
0	0.3806	0.3596	0.2992	0.2115	0.1241	0.0768	0.0718
2	0.3474	0.3283	0.2731	0.1930	0.1133	0.0701	0.0655
4	0.3175	0.3000	0.2496	0.1764	0.1035	0.0640	0.0599
(Madenci 2021)	0.3806	0.3596	0.2992	0.2115	0.1241	0.0768	0.0718

Table 16 The non-dimensional natural frequencies of CF CNTRC beams for FG-V distributions

μ	0º	15º	30º	45º	60º	75º	90º
0	0.3727	0.3520	0.2928	0.2071	0.1222	0.0766	0.0717
2	0.3402	0.3213	0.2673	0.1890	0.1115	0.0699	0.0654
4	0.3109	0.2936	0.2442	0.1727	0.1019	0.0639	0.0598
(Madenci 2021)	0.3727	0.3520	0.2928	0.2071	0.1222	0.0766	0.0717

Table 17 The non-dimensional natural frequencies of CF CNTRC beams for FG-O distributions

μ	0º	15º	30º	45º	60º	75º	90º
0	0.3710	0.3504	0.2913	0.2060	0.1215	0.0763	0.0716
2	0.3387	0.3199	0.2659	0.1880	0.1109	0.0696	0.0653
4	0.3095	0.2923	0.2430	0.1718	0.1013	0.0636	0.0597
(Madenci 2021)	0.3710	0.3504	0.2913	0.2060	0.1215	0.0763	0.0716

Table 18 The non-dimensional natural frequencies of CS CNTRC beams for UD distributions

μ	0º	15º	30º	45º	60º	75º	90º
0	1.2426	1.2021	1.0690	0.8250	0.5185	0.3305	0.3098
2	1.1344	1.0975	0.9759	0.7532	0.4733	0.3017	0.2828
4	1.0367	1.0029	0.8919	0.6883	0.4326	0.2757	0.2584
(Madenci 2021)	1.2426	1.2021	1.0690	0.8250	0.5185	0.3305	0.3098

Table 19 The non-dimensional natural frequencies of CS CNTRC beams for FG-X distributions

μ	0º	15º	30º	45º	60º	75º	90º
0	1.2525	1.2120	1.0789	0.8336	0.5235	0.3319	0.3107
2	1.1435	1.1065	0.9850	0.7610	0.4779	0.3030	0.2836
4	1.0450	1.0112	0.9001	0.6955	0.4367	0.2769	0.2592
(Madenci 2021)	1.2525	1.2120	1.0789	0.8336	0.5235	0.3319	0.3107

Table 20 The non-dimensional natural frequencies of CS CNTRC beams for FG-V distributions

μ	0º	15º	30º	45º	60º	75º	90º
0	1.2390	1.1981	1.0642	0.8203	0.5164	0.3308	0.3103
2	1.1312	1.0938	0.9716	0.7489	0.4714	0.3020	0.2833
4	1.0337	0.9996	0.8879	0.6844	0.4308	0.2760	0.2589
(Madenci 2021)	1.2390	1.1981	1.0642	0.8203	0.5164	0.3308	0.3103

Table 21 The non-dimensional natural frequencies of CS CNTRC beams for FG-O distributions

μ	0º	15º	30º	45º	60º	75º	90º
0	1.2344	1.1934	1.0594	0.8158	0.5133	0.3299	0.3098
2	1.1270	1.0895	0.9672	0.7448	0.4686	0.3011	0.2828
4	1.0299	0.9957	0.8839	0.6806	0.4282	0.2752	0.2584
(Madenci 2021)	1.2344	1.1934	1.0594	0.8158	0.5133	0.3299	0.3098

In the second section, we present the experimental results of FFNN. The specifications of the hardware and software used in the experiments are as follows: Windows 10 operating system, Intel(R) Core(TM) i5-3330 3.00 GHz, 4 GB of memory, visual studio 2017, C# programming language. In this study, the FFNN architecture has three layers (one input, one hidden, and one output). The numbers of neurons in the input and output layers are three and one, respectively. As mentioned above, the number of neurons in the hidden layer was started at two and was tried up to ten. Therefore, nine different FFNN architectures were used to determine the best model. The best model was found using the validation dataset and had nine neurons in the hidden layer. The best model has the architecture with 3-9-1. The momentum factor, the learning rate, and the maximum epoch number are 0.8, 0.3, and 1000, respectively. Eq. (41) shows the formulation of the generated best model. Table 22 shows the values of weights in the hidden layer of the generated best model. Table 23 shows the values of the weights and the biases in the output layer of the generated best model.

Table 22 The weights of the hidden layer

IHW		
0.1377	-13.8239	-0.4561
0.3644	-3.7677	2.5349
-0.0021	-3.2193	-2.9911
-0.3041	-1.8542	-2.4603
-1.0881	-2.2786	0.4406
0.6180	-2.9044	-0.1490
0.4843	0.4823	-2.4643
0.0049	0.1872	5.8122
-0.2262	5.2330	1.4390

Table 23 The biases in the hidden layer and the weights and the biases in the output layer

b_1	HOW	b_2
6.7103	9.0526	-1.2402
0.1532	-3.0927	
-0.1934	-3.4070	
-0.4038	-2.0494	
0.8941	-2.3713	
0.0879	-2.9252	
-0.4825	0.1584	
-2.9276	-4.1444	
-4.4383	5.6203	

Table 24 Performance of the generated FFNN model

Criteria	Training	Validation	Test
Instance	78	17	17
R	0.996	0.993	0.996
MAE	2.20E-02	2.72E-02	2.53E-02
MSE	7.18E-04	9.72E-04	9.08E-04

$$Y = sigmoid(sigmoid(X \times IHW + b_1) \times HOW + b_2) \quad (41)$$

where *sigmoid*(.) is the activation function, *X* represents the inputs. *IHW* and *HOW* represent the values of the weights in the hidden layer and output layer, respectively. b_1 and b_2 represent the values of the biases in the hidden layer and output layer, respectively.

Table 24 shows the performance results of the generated model for three sub-datasets. There are 112 instances in the dataset. The dataset is divided into 70% for training, 15% for validation, and 15% for test using stratified sampling in order to protect the class distribution as much as possible. Namely, 78 instances for training, 17 instances for validation, and 17 instances for test. Moreover, to eliminate the effect of the attributes in the dataset that have different scales, it is normalized using Eq. (36). The values of the correlation of the coefficient (R) for the training, validation, and test are 0.996, 0.9993, and 0.996, respectively. The

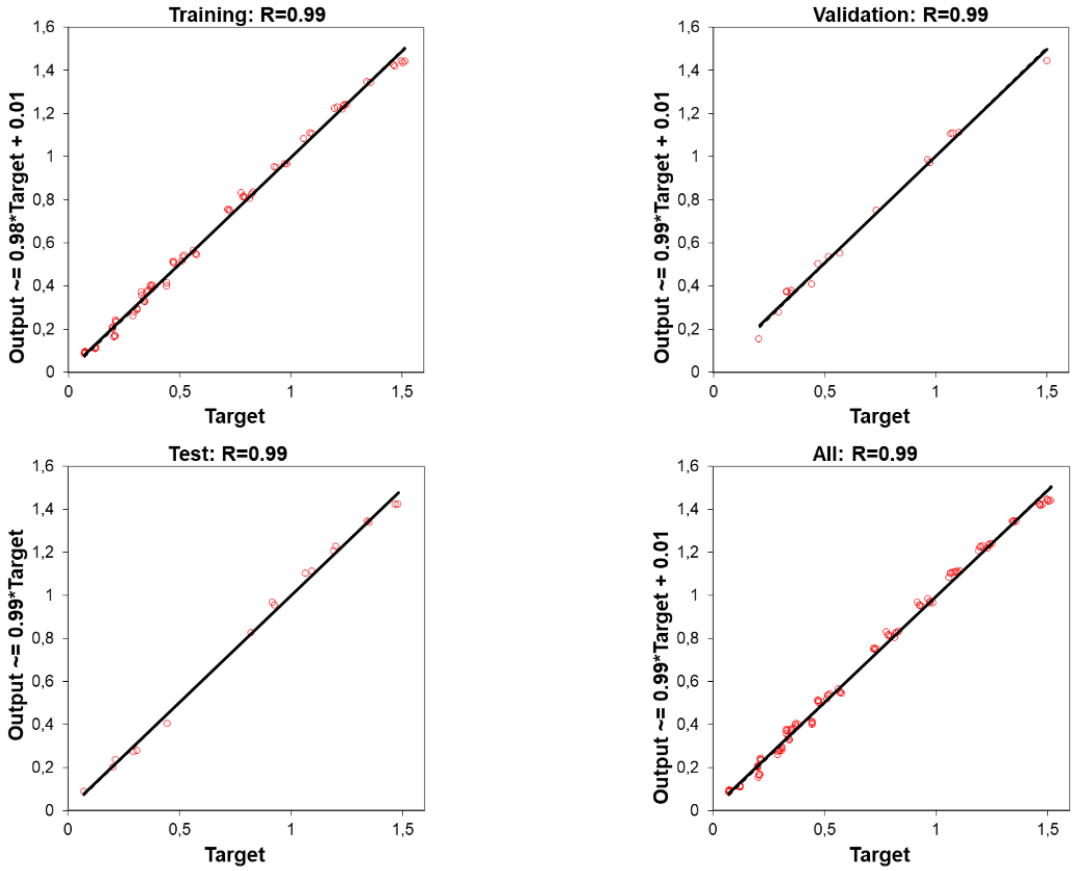

Fig. 2 The regression results of the training, validation, test, and all data

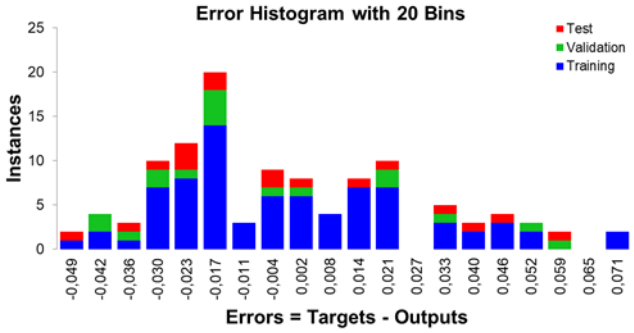

Fig. 3 The error histogram

larger the coefficient, the stronger the relationship, so that a correlation that is close to one indicates a very strong relationship, while coefficients that are near zero indicate very weak relationships (Bachman 2004). Because the values of the R for the training, validation, and test are very close to one, there is a very strong relationship. The values of the MAE for the training, validation and test are 2.20E-02, 2.72E-02, and 2.53E-02, respectively. The values of the MSE for the training, validation, and test are 7.18E-04, 9.72E-04, and 9.08E-04, respectively. Lower MSE and lower MAE indicate more accurate predictions. According to these results, the generated FFNN model has a good performance and accurate prediction.

The regression plots of the generated FFNN model are shown in Fig. 2. The prediction performance of the proposed FFNN model is very good according to the plots of the training, validation, test, and all data.

The error histogram of the generated FFNN model is shown in Fig. 3. It provides additional verification of the performance of the artificial neural network. It indicates outliers. The blue, green, and red areas represent training, validation, and test data respectively. Most data fall on zero error which provides an idea to check the outliers to determine if the data is bad, or if those data points are different than the rest of the data set. If the outliers are valid data points but are unlike the rest of the data, then the network is extrapolating for these points (Yadav et al. 2015). The density in the error histogram is around zero as shown in Fig. 3. Therefore, the prediction success of the generated FFNN model is very high.

4. Conclusions

In this study, an ANN-based model for the free vibration response of layered CNTRC beams was also presented. Dynamic characteristics of beams made up of FG-CNTRC nanobeams have been illustrated using the nonlocal classical beam theory. Nanobeams were considered to have a combination of FG-CNTRC layers with single-walled CNT. The effective material properties were obtained from the rule of the mixture by taking into account four types of volume distribution models using micromechanics theory.

The material properties of FG- CNTRCs are assumed to be graded through the thickness direction according to several distributions namely UD, FG-X, FG-V and FG-O. The main feature of the ANN is the learning ability from data. The main aim of this study is to develop a model which may predict the natural frequency. The proposed ANN model is composed of one input layer, one hidden layer, and one output layer. The architecture of the model is 3-9-1. In the experiments, we used 112 different data to predict the natural frequency using ANN. The input data in ANN are the CNT distribution models, boundary conditions, and fiber angels. The output data in ANN is the natural frequency. The train data are 70% of the data, the validation data are 15% of the data, and the test data are 15% of the data. The proposed ANN model is evaluated by the correlation of the coefficient (R), the mean absolute error (MAE), and the mean square error (MSE) statistical methods. The values of the R for the training, validation, and test are 0.996, 0.9993, and 0.996, respectively. Additionally, the values of the MAE and MSE are close to zero. In conclusion, the prediction ability of the ANN model is very good and the natural frequency can be predicted in ANN without attempting any experiments.

Ackowledgment

The research described in this paper was not financially supported.

References

Alajarmeh, O., X. Zeng, T. Aravinthan, T. Shelley, M. Alhawamdeh, A. Mohammed, L. Nicol, A. Vedernikov, A. Safonov and P. Schubel (2021), "Compressive behaviour of hollow box pultruded FRP columns with continuous-wound fibres", *Thin Wall. Struct.*, **168**, 108300. https://doi.org/10.1016/j.tws.2021.108300.

Aljarah, I., Faris, H. and Mirjalili, S. (2018), "Optimizing connection weights in neural networks using the whale optimization algorithm", *Soft Comput.*, **22**(1), 1-15. https://doi.org/10.1007/s00500-016-2442-1.

Asghar, S., Naeem, M.N., Hussain, M., Taj, M. and Tounsi, A. (2020), "Prediction and assessment of nonlocal natural frequencies of DWCNTs, Vibration analysis", *Comput. Concr.*, **25**(2), 133-144. https://doi.org/10.12989/cac.2020.25.2.133.

Asghar, S., Naeem, M.N., Khadimallah, M.A., Hussain, M., Iqbal, Z. and Tounsi, A. (2020), "Effect of chiral structure for free vibration of DWCNTs, Modal analysis", *Adv. Concr. Constr.*, **9**(6), 577-588. https://doi.org/10.12989/acc.2020.9.6.577.

Aydogdu, M. (2012), "Axial vibration analysis of nanorods (carbon nanotubes) embedded in an elastic medium using nonlocal elasticity", *Mech. Res. Commun.*, **43**, 34-40. https://doi.org/10.1016/j.mechrescom.2012.02.001.

Babaei, H., Y. Kiani and M.R. Eslami (2021), "Vibrational behavior of thermally pre-/post-buckled FG-CNTRC beams on a nonlinear elastic foundation, a two-step perturbation technique", *Acta Mech.*, **232**, 3897-3915. https://doi.org/10.1007/s00707-021-03027-z.

Bachman, L.F. (2004), Statistical analyses for language assessment book, Cambridge University Press.

Bebis, G. and Georgiopoulos, M. (1994), "Feed-forward neural networks", *IEEE Potentials*, **13**(4), 27-31. https://doi.org/10.1109/45.329294.

Bensaid, I. and Guenanou, A. (2017), "Bending and stability analysis of size-dependent compositionally graded Timoshenko nanobeams with porosities", *Adv. Mater. Res.*, **6**(1), 45. https://doi.org/10.12989/amr.2017.6.1.045.

Bouadi, A., Bousahla, A.A., Houari, M.S.A., Heireche, H. and Tounsi, A. (2018), "A new nonlocal HSDT for analysis of stability of single layer graphene sheet", *Adv. Nano Res.*, **6**(2), 147. https://doi.org/10.12989/anr.2018.6.2.147.

Bounouara, F., Benrahou, K.H., Belkorissat, I. and Tounsi, A. (2016), "A nonlocal zeroth-order shear deformation theory for free vibration of functionally graded nanoscale plates resting on elastic foundation", *Steel Compos. Struct.*, **20**(2), 227-249. https://doi.org/10.12989/scs.2016.20.2.227.

Bourada, F., Bousahla, A.A., Tounsi, A., Bedia, E., Mahmoud, S., Benrahou, K.H. and Tounsi, A. (2020), "Stability and dynamic analyses of SW-CNT reinforced concrete beam resting on elastic-foundation", *Comput. Concr.*, **25**(6), 485-495. https://doi.org/10.12989/cac.2020.25.6.485.

Bre, F., Gimenez, J.M. and Fachinotti, V.D. (2018), "Prediction of wind pressure coefficients on building surfaces using artificial neural networks", *Energy Build.*, **158**, 1429-1441. https://doi.org/10.1016/j.enbuild.2017.11.045.

Chavan, S.G. and Lal, A. (2018), "Geometrical nonlinear bending characteristics of SWCNTRC doubly curved shell panels", *Adv. Aircr. Spacecr. Sci.*, **5**(1), 21. https://doi.org/10.12989/aas.2018.5.1.021.

Dorffner, G. (1996), "Neural networks for time series processing", Neural Network World, 6, 447-468.

Duc, N.D., Seung-Eock, K., Quan, T.Q., Long, D.D. and Anh, V.M. (2018), "Nonlinear dynamic response and vibration of nanocomposite multilayer organic solar cell", *Compos. Struct.*, **184**, 1137-1144. https://doi.org/10.1016/j.compstruct.2017.10.064.

Eberhardt, O. and Wallmersperger, T. (2015), "Energy consistent modified molecular structural mechanics model for the determination of the elastic properties of single wall carbon nanotubes", *Carbon*, **95**, 166-180. https://doi.org/10.1016/j.carbon.2015.07.092.

Ebrahimi, F. and Barati, M.R. (2016), "An exact solution for buckling analysis of embedded piezo-electro-magnetically actuated nanoscale beams", *Adv. Nano Res.*, **4**(2), 65. https://doi.org/10.12989/anr.2016.4.2.065.

Ebrahimi, F. and Barati, M.R. (2018), "Stability analysis of functionally graded heterogeneous piezoelectric nanobeams based on nonlocal elasticity theory", *Adv. Nano Res.*, **6**(2), 93. https://doi.org/10.12989/anr.2018.6.2.093.

Ebrahimi, F. and Farazmandnia, N. (2018), "Vibration analysis of functionally graded carbon nanotube-reinforced composite sandwich beams in thermal environment", *Adv. Aircr. Spacecr. Sci.*, **5**(1), 107. https://doi.org/10.12989/aas.2018.5.1.107.

Ehyaei, J. and M. Daman (2017), "Free vibration analysis of double walled carbon nanotubes embedded in an elastic medium with initial imperfection", *Adv. Nano Res.*, **5**(2), 179. https://doi.org/10.12989/anr.2017.5.2.179

Eldem, A. (2020), "An application of deep neural network for classification of wheat seeds", *Eur. J. Sci. Technol.*, **19**, 213-220. https://doi.org/10.31590/ejosat.719048.

Eltaher, M., Khater, M., Park, S., Abdel-Rahman, E. and Yavuz, M. (2016), "On the static stability of nonlocal nanobeams using higher-order beam theories", *Adv. Nano Res.*, **4**(1), 51-64. https://doi.org/10.12989/anr.2016.4.1.051.

Eltaher, M.A., Almalki, T.A., Ahmed, K.I. and Almitani, K.H. (2019), "Characterization and behaviors of single walled carbon nanotube by equivalent-continuum mechanics approach", *Adv. Nano Res.*, **7**(1), 39-49. https://doi.org/10.12989/anr.2019.7.1.039.

Eringen, A.C. (1983), "On differential equations of nonlocal elasticity and solutions of screw dislocation and surface waves", *J. Appl. Phys.*, **54**(9), 4703-4710. https://doi.org/10.1063/1.332803.

Farazin, A. and Mohammadimehr, M. (2021), "Computer modeling to forecast accurate of efficiency parameters of different size of graphene platelet, carbon, and boron nitride nanotubes, A molecular dynamics simulation", *Comput. Concr.*, **27**(2), 111-130. https://doi.org/10.12989/cac.2021.27.2.111.

Frimpong, E.A., Oluwasanmi, A., Baagyere, E.Y. and Zhiguang, Q. (2021), "A feedforward artificial neural network model for classification and detection of type 2 diabetes", *J. Phys.*, **1734**(1), 012026. https://doi.org/10.1088/1742-6596/1734/1/012026.

Ghadyani, G., Soufeiani, L. and Öchsner, A. (2016), "On the characterization of the elastic properties of asymmetric single-walled carbon nanotubes", *J. Phys. Chem. Solid.*, **89**, 62-68. https://doi.org/10.1016/j.jpcs.2015.10.013.

Gülcü, Ş. (2020), "Training of the artificial neural networks using states of matter search algorithm", *Int. J. Intell. Syst. Appl. Eng.*, **8**(3), 131-136. https://doi.org/10.18201/ijisae.2020363532.

Gülcü, Ş. (2021), "An improved animal migration optimization algorithm to train the feed-forward artificial neural networks", *Arab. J. Sci. Eng.*, 1-25. https://doi.org/10.1007/s13369-021-06286-z.

Hacibeyoglu, M. and Ibrahim, M.H. (2018), "Human gender prediction on facial mobil images using convolutional neural networks", *Int. J. Intell. Syst. Appl. Eng.*, **6**(3), 203-208. https://doi.org/10.18201/ijisae.2018644778.

Hakim, S. and Razak, H.A. (2013), "Structural damage detection of steel bridge girder using artificial neural networks and finite element models", *Steel Compos. Struct.*, **14**(4), 367-377. https://doi.org/10.12989/scs.2013.14.4.367.

Hosseini, S., Moghaddam, M. and Rahmani, O. (2020), "Exact solution for axial vibration of the power, exponential and sigmoid FG nonlocal nanobeam", *Adv. Aircr. Spacecr. Sci.*, **7**(6), 517-536. https://doi.org/10.12989/aas.2020.7.6.517.

Hosseini, S.A. and Khosravi, F. (2020), "Exact solution for dynamic response of size dependent torsional vibration of CNT subjected to linear and harmonic loadings", *Adv. Nano Res.*, **8**(1), 25-36. https://doi.org/10.12989/anr.2020.8.1.025.

Hussain, M., Naeem, M.N., Asghar, S. and Tounsi, A. (2020a), "Theoretical impact of Kelvin's theory for vibration of double walled carbon nanotubes", *Adv. Nano Res.*, **8**(4), 307-322. https://doi.org/10.12989/anr.2020.8.4.307.

Hussain, M., Naeem, M.N. and Tounsi, A. (2020b), "Numerical Study for nonlocal vibration of orthotropic SWCNTs based on Kelvin's model", *Adv. Concr. Constr.*, **9**(3), 301-312. https://doi.org/10.12989/acc.2020.9.3.301.

Hussain, M., Naeem, M.N. and Tounsi, A. (2020c), "Response of orthotropic Kelvin modeling for single-walled carbon nanotubes, Frequency analysis", *Adv. Nano Res.*, **8**(3), 229-244. https://doi.org/10.12989/anr.2020.8.3.229.

Jam, J.E. and Y. Kiani (2015), "Low velocity impact response of functionally graded carbon nanotube reinforced composite beams in thermal environment", *Compos. Struct.*, **132**, 35-43. https://doi.org/10.1016/j.compstruct.2015.04.045.

James, G., Witten, D., Hastie, T. and Tibshirani, R. (2013), An introduction to statistical learning, Springer.

Kannan, S., Kim, B., Gupta, A., Noh, S.H. and Li, L. (2012), "Characterization of high performance CNT-based TSV for high-frequency RF applications", *Adv. Mater. Res.*, **1**(1), 37. https://doi.org/10.12989/amr.2012.1.1.037.

Karami, B., Janghorban, M. and Tounsi, A. (2018), "Nonlocal strain gradient 3D elasticity theory for anisotropic spherical nanoparticles", *Steel Compos. Struct.*, **27**(2), 201-216. https://doi.org/10.12989/scs.2018.27.2.201.

Karaşahin, A.T. and Tümer, A.E. "Real time traffic signal timing approach based on artificial neural network", *MANAS J. Eng.*, **8**(1), 49-54.

Khaniki, H.B. and M.H. Ghayesh (2020), "A review on the mechanics of carbon nanotube strengthened deformable structures", *Eng. Struct.*, **220**, 110711. https://doi.org/10.1016/j.engstruct.2020.110711

Khater, H. and Abd el Gawaad, H. (2016), "Characterization of alkali activated geopolymer mortar doped with MWCNT", *Constr. Build. Mater.*, **102**, 329-337. https://doi.org/10.1016/j.conbuildmat.2015.10.121.

Kheroubi, B., Benzair, A., Tounsi, A. and Semmah, A. (2016), "A new refined nonlocal beam theory accounting for effect of thickness stretching in nanoscale beams", *Adv. Nano Res.*, **4**(4), 251. https://doi.org/10.12989/anr.2016.4.4.251.

Khosravi, F. and Hosseini, S.A. (2020), "On the viscoelastic carbon nanotube mass nanosensor using torsional forced vibration and Eringen's nonlocal model", *Mech. Based Des. Struct.*, 1-24. https://doi.org/10.1080/15397734.2020.1744001.

Khosravi, S., H. Arvin and Y. Kiani (2019a), "Interactive thermal and inertial buckling of rotating temperature-dependent FG-CNT reinforced composite beams", *Compos. Part B Eng.*, **175**, 107178. https://doi.org/10.1016/j.compositesb.2019.107178

Khosravi, S., H. Arvin and Y. Kiani (2019b), "Vibration analysis of rotating composite beams reinforced with carbon nanotubes in thermal environment", *Int. J. Mech. Sci.*, **164**, 105187. https://doi.org/10.1016/j.ijmecsci.2019.105187

Kiani, Y. (2016), "Thermal postbuckling of temperature-dependent sandwich beams with carbon nanotube-reinforced face sheets", *J. Therm. Stress.*, **39**(9), 1098-1110. https://doi.org/10.1080/01495739.2016.1192856.

Kohonen, T. (1982), "Self-organized formation of topologically correct feature maps", *Biol. Cybernet.*, **43**(1), 59-69. https://doi.org/10.1007/BF00337288.

Korotkov, R., A. Vedernikov, S. Gusev, O. Alajarmeh, I. Akhatov and A. Safonov (2021), "Shape memory behavior of unidirectional pultruded laminate", *Compos. Part A Appl. Sci.*, **150**, 106609. https://doi.org/10.1016/j.compositesa.2021.106609.

Kumar, B.R. (2018), "Investigation on mechanical vibration of double-walled carbon nanotubes with inter-tube Van der waals forces", *Adv. Nano Res.*, **6**(2), 135. https://doi.org/10.12989/anr.2018.6.2.135.

Madenci, E. (2021), "Free vibration analysis of carbon nanotube RC nanobeams with variational approaches", *Adv. Nano Res.*, **11**(2), 157-171. https://doi.org/10.12989/anr.2021.11.2.157.

Madenci, E. (2023), "Fonksiyonel Derecelendirilmiş Malzeme Plakların Statik Analizinde Mikro-Mekanik Modellerin Katkısı", *Necmettin Erbakan Üniversitesi Fen ve Mühendislik Bilimleri Dergisi*, **5**(1), 23-37. https://doi.org/10.47112/neufmbd.2023.7.

Madenci, E. and Gülcü, Ş. (2020), "Optimization of flexure stiffness of FGM beams via artificial neural networks by mixed FEM", *Struct. Eng. Mech.*, **75**(5), 633-642. https://doi.org/10.12989/sem.2020.75.5.633.

Madenci, E., Özkılıç, Y.O., Hakamy, A. and Tounsi, A. (2023), "Experimental tensile test and micro-mechanic investigation on carbon nanotube reinforced carbon fiber composite beams", *Adv. Nano Res.*, **14**(5), 443-450. https://doi.org/10.12989/anr.2023.14.5.443

Mehar, K., Panda, S.K., Dehengia, A. and Kar, V.R. (2016), "Vibration analysis of functionally graded carbon nanotube reinforced composite plate in thermal environment", *J. Sandw. Struct. Mater.*, **18**(2), 151-173. https://doi.org/10.1177/1099636215613324.

Mirjalili, S. (2015), "How effective is the Grey Wolf optimizer in training multi-layer perceptrons", *Appl. Intell.*, **43**(1), 150-161. https://doi.org/10.1007/s10489-014-0645-7.

Mirzaei, M. and Y. Kiani (2015), "Snap-through phenomenon in a thermally postbuckled temperature dependent sandwich beam with FG-CNTRC face sheets", *Compos. Struct.*, **134**, 1004-1013. https://doi.org/10.1016/j.compstruct.2015.09.003.

Mirzaei, M. and Y. Kiani (2016), "Nonlinear free vibration of temperature-dependent sandwich beams with carbon nanotube-reinforced face sheets", *Acta Mech.*, **227**(7), 1869-1884. https://doi.org/10.1007/s00707-016-1593-6.

Mokhtar, Y., Heireche, H., Bousahla, A.A., Houari, M.S.A., Tounsi, A. and Mahmoud, S. (2018), "A novel shear deformation theory for buckling analysis of single layer graphene sheet based on nonlocal elasticity theory", *Smart Struct. Syst.*, **21**(4), 397-405. https://doi.org/10.12989/sss.2018.21.4.397.

Mouffoki, A., Bedia, E.A., Houari, M.S.A., Tounsi, A. and Mahmoud, S. (2017), "Vibration analysis of nonlocal advanced nanobeams in hygro-thermal environment using a new two-unknown trigonometric shear deformation beam theory", *Smart Struct. Syst.*, **20**(3), 369-383. https://doi.org/10.12989/sss.2017.20.3.369.

Park, J. and Sandberg, I.W. (1993), "Approximation and radial-basis-function networks", *Neural Comput.*, **5**(2), 305-316. https://doi.org/10.1162/neco.1993.5.2.305.

Qin, B., Zhong, R., Wang, T., Wang, Q., Xu, Y. and Hu, Z. (2020), "A unified Fourier series solution for vibration analysis of FG-CNTRC cylindrical, conical shells and annular plates with arbitrary boundary conditions", *Compos. Struct.*, **232**, 111549. https://doi.org/10.1016/j.compstruct.2019.111549.

Shekari, A., Ghasemi, F.A. and Malekzadehfard, K. (2017), "Free damped vibration of rotating truncated conical sandwich shells using an improved high-order theory", *Latin Am. J. Solids Struct.*, **14**(12), 2291-2323. https://doi.org/10.1590/1679-78253977.

Shen, H.S., Li, C. and Reddy, J.N. (2020), "Large amplitude vibration of FG-CNTRC laminated cylindrical shells with negative Poisson's ratio", *Comput. Methods Appl. Mech. Eng.*, **360**, 112727. https://doi.org/10.1016/j.cma.2019.112727.

Şimşek, M. and Yurtcu, H.H. (2013), "Analytical solutions for bending and buckling of functionally graded nanobeams based on the nonlocal Timoshenko beam theory", *Compos. Struct.*, **97**, 378-386. https://doi.org/10.1016/j.compstruct.2012.10.038.

Thai, H.T. and Vo, T.P. (2012), "A nonlocal sinusoidal shear deformation beam theory with application to bending, buckling, and vibration of nanobeams", *Int. J. Eng. Sci.*, **54**, 58-66. https://doi.org/10.1016/j.ijengsci.2012.01.009.

Tounsi, A., Houari, M.S.A. and Benyoucef, S. (2013), "A refined trigonometric shear deformation theory for thermoelastic bending of functionally graded sandwich plates", *Aerosp. Sci. Technol.*, **24**(1), 209-220. https://doi.org/10.1016/j.ast.2011.11.009.

Tümer, A., Edebali, S. and Gülcü, Ş. (2020), "Modeling of Removal of Chromium (VI) from Aqueous Solutions Using Artificial Neural Network", *Iran. J. Chem. Chem. Eng.*, **39**(1), 163-175. https://doi.org/10.30492/ijcce.2020.33257.

Uyaner, M. and A. Yar (2019), "Nano Elyaf Takviyeli Nanokompozit Üretimi ve Karakterizasyonu", *Necmettin Erbakan Üniversitesi Fen ve Mühendislik Bilimleri Dergisi*, **1**(1), 10-19.

Vedernikov A, Safonov A, Tucci F, Carlone P, Akhatov I. (2020), "Pultruded materials and structures: A review", *J. Compos. Mater.*, **54**(26), 4081-4117. https://doi.org/10.1177/0021998320922894

Wang, Y.Z., H.T. Cui, F.M. Li and K. Kishimoto (2011), "Effects of viscous fluid on wave propagation in carbon nanotubes", *Phys. Lett. A*, **375**(24), 2448-2451. https://doi.org/10.1016/j.physleta.2011.05.016

Wang, Y.Z., F.M. Li and K. Kishimoto (2010), "Wave propagation characteristics in fluid-conveying double-walled nanotubes with scale effects", *Comput. Mater. Sci.*, **48**(2), 413-418. https://doi.org/10.1016/j.commatsci.2010.01.034

Wang, Y.Z. and F.M. Li (2014), "Nonlinear free vibration of nanotube with small scale effects embedded in viscous matrix", *Mech. Res. Commun.*, **60**, 45-51. https://doi.org/10.1016/j.mechrescom.2014.06.002

Wang, Y.Z., F.M. Li and K. Kishimoto (2012), "Effects of axial load and elastic matrix on flexural wave propagation in nanotube with nonlocal Timoshenko beam model", *J. Vib. Acoust.*, **134**(3), 031011. https://doi.org/10.1115/1.4005832

Wu, H., Kitipornchai, S. and Yang, J. (2015), "Free vibration and buckling analysis of sandwich beams with functionally graded carbon nanotube-reinforced composite face sheets", *Int. J. Struct. Stabil. Dyn.*, **15**(7), 1540011. https://doi.org/10.1142/S0219455415400118.

Yadav, A.K., Malik, H. and Mittal, A. (2015), "Artificial neural network fitting tool based prediction of solar radiation for identifying solar power potential", *J. Electr. Eng.*, **15**(2), 25-29.

Youcef, D.O., Kaci, A., Benzair, A., Bousahla, A.A. and Tounsi, A. (2018), "Dynamic analysis of nanoscale beams including surface stress effects", *Smart Struct. Syst.*, **21**(1), 65-74. https://doi.org/10.12989/sss.2018.21.1.065.

AT